DE GRUYTER OPEN

Acta Geophysica
vol. 64, no. 3, June 2016, pp. 732-754
DOI: 10.1515/acgeo-2016-0019

Accurate Establishment of Error Models for the Satellite Gravity Gradiometry Recovery and Requirements Analysis for the Future GOCE Follow-On Mission

Wei ZHENG[1,2], Zhaokui WANG[3], Yanwei DING[4], and Zhaowei LI[1]

[1]Qian Xuesen Laboratory of Space Technology, China Academy of Space Technology, Beijing, China; e-mail: zhengwei1@qxslab.cn

[2]State Key Laboratory of Geodesy and Earth's Dynamics, Institute of Geodesy and Geophysics, Chinese Academy of Sciences, Wuhan, China; e-mail: wzheng@asch.whigg.ac.cn

[3]School of Aerospace Engineering, Tsinghua University, Beijing, China

[4]Aerospace Dongfanghong Satellite Company Limited, Beijing, China

Abstract

Firstly, the new single and combined error models applied to estimate the cumulative geoid height error are efficiently produced by the dominating error sources consisting of the gravity gradient of the satellite-equipped gradiometer and the orbital position of the space-borne GPS/GLONASS receiver using the power spectral principle. At degree 250, the cumulative geoid height error is 1.769×10^{-1} m based on the new combined error model, which preferably accords with a recovery accuracy of 1.760×10^{-1} m from the GOCE-only Earth gravity field model GO_CONS_GCF_2_TIM_R2 released in Germany. Therefore, the new combined error model of the cumulative geoid height is correct and reliable in this study. Secondly, the requirements analysis for the future GOCE Follow-On satellite system is carried out in respect of the preferred design of the matching measurement accuracy of key payloads comprising the gravity gradient and orbital position and the optimal selection of the orbital altitude of the satellite. We recommend the gravity gradient with an accuracy of 10^{-13}-10^{-15} /s^2, the orbital position with a precision of 1-0.1 cm and the orbital altitude of 200-250 km in the future GOCE Follow-On mission.

Key words: GOCE Follow-On, single and combined error models, requirements analysis, power spectral principle, satellite gravity gradiometry recovery.

1. INTRODUCTION

The successful implementation of the satellite gravity gradiometry (SGG) mission is another breakthrough innovation in the interdisciplinary scientific fields, *e.g.*, space geodesy, geophysics, *etc*., after the Global Positioning System (GPS) is constructed by the U.S. Department of Defense (DOD) (Hsu 2001). The European Space Agency (ESA) independently developed and successfully launched the Gravity Field and Steady-State Ocean Circulation Explorer (GOCE) satellite on 17 March 2009. As shown in Table 1, the GOCE satellite flies in an almost-circular, sun-synchronous and low-altitude orbit, and adopts a combination of the Satellite-to-Satellite Tracking in the High-Low mode (Zheng *et al.* 2011a, 2012a,b, 2015a) with the Satellite Gravity Gradiometry mode (SST-HL/SGG). Apart from the accurate tracking and positioning of the low-orbiting GOCE satellite by the high-orbit

Table 1

A comparison of the current GOCE and future GOCE Follow-On mission

Parameters		Gravity satellites	
		GOCE	GOCE Follow-On
Orbit	Orbital altitude	250 km	200-250 km
	Orbital inclination	96.5°	90–95°
	Orbital eccentricity	10^{-3}	10^{-3}–10^{-4}
	Tracking model	SST-HL/SGG	SST-HL/SGG
Payload	Gravity gradient error	3×10^{-12} /s^2 (Electrostatic suspension gravity gradiometer)	10^{-13}–10^{-15} /s^2 (Cold-atom interferometric gravity gradiometer)
	Orbital position error	1 cm (GPS/GLONASS)	1-0.1 cm (GPS/GLONASS/ Compass/Galileo)

GPS/GLONASS system (Bobojc and Drozyner 2011), the second-derivatives of the Earth's gravitational potential at the satellite orbit are precisely measured through the space-based electrostatic suspension gravity gradiometer located at the center of mass of the GOCE satellite (Bian and Ji 2006, Eshagh 2010), and the non-conservative forces acting on the GOCE system are compensated in real time by the satellite-borne Drag-Free Control System (DFCS).

At present, the recovery methods for the satellite gravity gradiometry mainly include the space-wise method (Reguzzoni and Tselfes 2009, Migliaccio *et al.* 2010, 2011; Pertusini *et al.* 2010, Reguzzoni *et al.* 2010, Sanso *et al.* 2011, Liu *et al.* 2012), the time-wise method (Milani *et al.* 2005, Pail *et al.* 2010, 2011a; Eshagh 2011, Goiginger *et al.* 2011), the space-time-wise method (Zheng *et al.* 2011b), and the direct method (Bruinsma *et al.* 2010, Pail *et al.* 2011b), and so on. On 10 November 2013, the GOCE satellite has ended its extended mission to map the Earth's gravitational field. As displayed in Table 1, many international research organizations are actively carrying through the intensive and extensive investigations concerning the requirements analysis and payload development for the future GOCE Follow-On satellite mission (Bender *et al.* 2003, Rummel 2003, Zheng *et al.* 2012c, 2013, 2015b) for the sake of meeting the urgent requirements for the related interdisciplines on further improving the accuracy of the Earth's gravitational field determination. In the interest of efficiently getting rid of the existing shortcomings containing the complex computational process, slow computing speed, *etc*., in the current methods for the satellite gravity gradiometry recovery, we first founded the single and combined error models for the gravity recovery depending on the errors in gravity gradient measurements of the satellite-equipped gravity gradiometer and the errors in orbital position observations of the satellite-borne GPS/GLONASS receiver by the power spectral principle (Welch 1967, Jenkins and Watts 1968, Press *et al.* 1992a, b), and proposed the matching accuracy indexes of the pivotal sensors and the appropriate orbital parameter of the satellite for the future GOCE Follow-On mission.

2. POWER SPECTRUM OF GRAVITY GRADIENT SIGNALS

The spherical harmonic series expansion of the Earth's gravitational potential in the Earth-fixed coordinate system is defined as (Ditmar *et al*. 2003)

$$V\left(r,\theta,\lambda\right)=\frac{GM}{R_{\mathrm{e}}}\sum_{l=0}^{L}\left(\frac{\mathrm{R}_{\mathrm{e}}}{r}\right)^{l+1}\sum_{m=0}^{l}\left(\overline{C}_{lm}\cos m\lambda+\overline{S}_{lm}\sin m\lambda\right)\overline{\mathrm{P}}_{lm}\left(\cos\theta\right)\ , \tag{1}$$

where GM is the product of the gravitational constant G and the Earth's mass M; R_{e} denotes the mean radius of the Earth; L represents the maximum de-

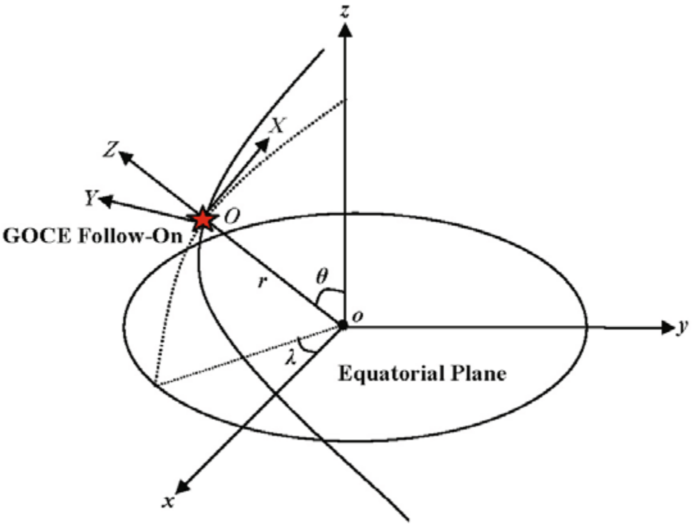

Fig. 1. Local North-Stabilized (LNS) frame *O-XYZ* and Earth-Centered Inertial (ECI) frame *o-xyz*.

gree of the spherical harmonic expansion; r, θ, and λ are the geocentric radius, geocentric colatitude and geocentric longitude, respectively; $\overline{\mathrm{P}}_{lm}(\cos\theta)$ indicates the normalized associated Legendre polynomials of degree l and order m; and $\overline{C}_{lm}, \overline{S}_{lm}$ express the estimated normalized geopotential coefficients.

As shown in Fig. 1, the transformation formula between the Local North-Stabilized (LNS) frame (X, Y, Z) and the Earth-Centered Inertial (ECI) frame (x, y, z) can be given by

$$\begin{bmatrix} x \\ y \\ z \end{bmatrix} = \begin{bmatrix} -\cos(\pi-\lambda)\cos(\pi/2+\theta) & \sin(\pi-\lambda) & \cos(\pi-\lambda)\sin(\pi/2+\theta) \\ -\sin(\pi-\lambda)\cos(\pi/2+\theta) & -\cos(\pi-\lambda) & \sin(\pi-\lambda)\sin(\pi/2+\theta) \\ \sin(\pi/2+\theta) & 0 & \cos(\pi/2+\theta) \end{bmatrix} \begin{bmatrix} X \\ Y \\ Z+r \end{bmatrix}. \quad (2)$$

O-XYZ represents the local north-stabilized frame, where the origin O is located at the center of mass of the satellite, the X- and Y-axis are respectively directed to the north and west, and the Z-axis completes a right-handed triad with X- and Y-axis. Analytic formulas for the second-order derivatives of the Earth's gravitational potentials $V(r, \theta, \lambda)$ at a point with spherical coordinates (r, θ, λ) are greatly simple in the local north-stabilized frame (Moritz 1971, Tscherning 1976). The second-order gradients of $V(r, \theta, \lambda)$ with respect to X, Y, Z in the local north-stabilized frame yields

$$\Gamma=\begin{bmatrix} V_{XX} & V_{XY} & V_{XZ} \\ V_{YX} & V_{YY} & V_{YZ} \\ V_{ZX} & V_{ZY} & V_{ZZ} \end{bmatrix}, \tag{3}$$

where Γ is a symmetrical traceless matrix, $V_{XX}+V_{YY}+V_{ZZ}=0$, with five independent components of nine gravity gradient tensors

$$\begin{cases} \boldsymbol{V}_{XX}(r,\theta,\lambda)=\dfrac{GM}{R_{\mathrm{e}}^3}\sum_{l=2}^{L}(\dfrac{R_{\mathrm{e}}^3}{r})^{l+3}\sum_{m=0}^{l}(\bar{\boldsymbol{C}}_{lm}\cos m\lambda+\bar{\boldsymbol{S}}_{lm}\sin m\lambda)\boldsymbol{H}^{XX}(\theta) \\ \boldsymbol{V}_{YY}(r,\theta,\lambda)=\dfrac{GM}{R_{\mathrm{e}}^3}\sum_{l=2}^{L}(\dfrac{R_{\mathrm{e}}^3}{r})^{l+3}\sum_{m=0}^{l}(\bar{\boldsymbol{C}}_{lm}\cos m\lambda+\bar{\boldsymbol{S}}_{lm}\sin m\lambda)\boldsymbol{H}^{YY}(\theta) \\ \boldsymbol{V}_{ZZ}(r,\theta,\lambda)=\dfrac{GM}{R_{\mathrm{e}}^3}\sum_{l=2}^{L}\left(\dfrac{R_{\mathrm{e}}^3}{r}\right)^{l+3}\sum_{m=0}^{l}\left(\bar{\boldsymbol{C}}_{lm}\cos m\lambda+\bar{\boldsymbol{S}}_{lm}\sin m\lambda\right)\boldsymbol{H}^{ZZ}(\theta) \\ \boldsymbol{V}_{XY}(r,\theta,\lambda)=\dfrac{GM}{R_{\mathrm{e}}^3}\sum_{l=2}^{L}\left(\dfrac{R_{\mathrm{e}}^3}{r}\right)^{l+3}\sum_{m=0}^{l}\left(-\bar{\boldsymbol{C}}_{lm}\sin m\lambda+\bar{\boldsymbol{S}}_{lm}\cos m\lambda\right)\boldsymbol{H}^{XY}(\theta) \\ \boldsymbol{V}_{XZ}(r,\theta,\lambda)=\dfrac{GM}{R_{\mathrm{e}}^3}\sum_{l=2}^{L}\left(\dfrac{R_{\mathrm{e}}^3}{r}\right)^{l+3}\sum_{m=0}^{l}\left(\bar{\boldsymbol{C}}_{lm}\cos m\lambda+\bar{\boldsymbol{S}}_{lm}\sin m\lambda\right)\boldsymbol{H}^{XZ}(\theta) \\ \boldsymbol{V}_{YZ}(r,\theta,\lambda)=\dfrac{GM}{R_{\mathrm{e}}^3}\sum_{l=2}^{L}\left(\dfrac{R_{\mathrm{e}}^3}{r}\right)^{l+3}\sum_{m=0}^{l}\left(-\bar{\boldsymbol{C}}_{lm}\sin m\lambda+\bar{\boldsymbol{S}}_{lm}\cos m\lambda\right)\boldsymbol{H}^{YZ}(\theta) \end{cases}, \tag{4}$$

where

$$\begin{cases} \boldsymbol{H}^{XX}(\theta)=\bar{\boldsymbol{P}}_{lm}''(\cos\theta)-(l+1)\bar{\boldsymbol{P}}_{lm}(\cos\theta) \\ \boldsymbol{H}^{YY}(\theta)=\tan^{-1}\theta\bar{\boldsymbol{P}}_{lm}'(\cos\theta)-\left(l+1+m^2\sin^{-2}\theta\right)\bar{\boldsymbol{P}}_{lm}(\cos\theta) \\ \boldsymbol{H}^{ZZ}(\theta)=(l+1)(l+2)\bar{\boldsymbol{P}}_{lm}(\cos\theta) \\ \boldsymbol{H}^{XY}(\theta)=m\sin^{-1}\theta\left[\bar{\boldsymbol{P}}_{lm}'(\cos\theta)-\tan^{-1}\theta\bar{\boldsymbol{P}}_{lm}(\cos\theta)\right] \\ \boldsymbol{H}^{XZ}(\theta)=(l+2)\bar{\boldsymbol{P}}_{lm}'(\cos\theta) \\ \boldsymbol{H}^{YZ}(\theta)=m(l+2)\sin^{-1}\theta\bar{\boldsymbol{P}}_{lm}(\cos\theta) \end{cases}$$

the zero-order, first-order, and second-order derivatives of the Legendre functions are, respectively, represented as

$$\begin{cases} \bar{\boldsymbol{P}}_{lm}(\cos\theta)=\gamma_m 2^{-l}\sin^m\theta\sum_{k=0}^{[(l-m)/2]}(-1)^k\dfrac{(2l-2k)!}{k!(l-k)!(l-m-2k)!}(\cos\theta)^{l-m-2k} \qquad (m\le l) \\ \bar{\boldsymbol{P}}_{lm}'(\cos\theta)=\dfrac{1}{\sin\theta}\left[(l+1)\cos\theta\bar{\boldsymbol{P}}_{lm}(\cos\theta)-(l-m-1)\bar{\boldsymbol{P}}_{l+1,m}(\cos\theta)\right] \\ \bar{\boldsymbol{P}}_{lm}''(\cos\theta)=-l\bar{\boldsymbol{P}}_{lm}(\cos\theta)+l\cos\theta\bar{\boldsymbol{P}}_{l-1,m}'(\cos\theta)+\dfrac{l}{4}\cos^2\theta\left[\bar{\boldsymbol{P}}_{l-1,m+1}'(\cos\theta)-4\bar{\boldsymbol{P}}_{l-1,m-1}'(\cos\theta)\right] \end{cases}$$

where

$$\gamma_m = \begin{cases} \sqrt{2(2l+1)\dfrac{(l-|m|)!}{(l+|m|)!}} & (m \neq 0) \\ \sqrt{2l+1} & (m = 0) \end{cases} .$$

According to the Parseval's theorem of the spherical harmonic function, the power spectrum of the satellite gravity gradient V_{ab} in the local north-stabilized frame is denoted as

$$P^2\left(V_{ab}\right) = \frac{1}{4\pi} \iint \left[V_{ab}(r,\phi,\lambda)\right]^2 \cos\phi \mathrm{d}\phi \mathrm{d}\lambda \ , \tag{5}$$

where $a, b = X, Y, Z$.

Combining Eqs. 2, 4, and 5 and the orthogonality of the spherical harmonic function, the power spectrum of the gravity gradient signals in the Earth-centered inertial frame is indicated as (Meng and Liu 1993, van Gelderen and Koop 1997, Zheng *et al.* 2012c)

$$P^2\left(V_{ij}\right) = \left(\frac{GM}{R_e^3}\right)^2 \sum_{l=0}^{L} A_{ij}^2 \left(\frac{R_e}{R_e+H}\right)^{2l+6} \sum_{m=0}^{l} \left(\bar{C}_{lm}^2 + \bar{S}_{lm}^2\right) , \tag{6}$$

where A_{ij} is the sensitivity coefficient ($i, j = x, y, z$), H is the orbital altitude of the satellite, and $\bar{C}_{lm}, \bar{S}_{lm}$ are derived from the Earth gravity field model GO_CONS_GCF_2_TIM_R2 released by the Technical University of Munich (TUM), Germany (Pail *et al.* 2011a).

Based on Eq. 6, the total power spectrum $P^2(V_{xyz})$ of the gravity gradient tensor signals is represented as

$$P^2\left(V_{xyz}\right) = P^2\left(V_{xx}\right) + P^2\left(V_{yy}\right) + P^2\left(V_{zz}\right) + P^2\left(V_{xz}\right) , \tag{7}$$

where V_{xyz} denotes the total signals of the gravity gradient tensors consisting of V_{xx}, V_{yy}, V_{zz}, and V_{xz}.

By the Kaula's rule (Kaula 1966), the power spectrum $P_{\mathrm{K}}^2(V_{ij})$ of the satellite gravity gradient tensor signals is shown as

$$P_{\mathrm{K}}^2\left(V_{ij}\right) = \left(\frac{GM}{R_e^3}\right)^2 \sum_{l=0}^{L} A_{ij}^2 \left(\frac{R_e}{R_e+H}\right)^{2l+6} (2l+1)\frac{10^{-10}}{l^4} , \tag{8}$$

where the subscript K means "Kaula's rule" in $P_{\mathrm{K}}^2(V_{ij})$.

Table 2

Sensitivity coefficients of power spectrum from satellite gravity gradient tensors

Power spectrum of gradients	Sensitivity coefficients A_{ij}
$P^2(V_{xx})$	$A_{xx} = -\sqrt{\dfrac{(l+1)^3(l+2)(2l+3)}{3(2l+1)}}$
$P^2(V_{yy})$	$A_{yy} = -\left[(l+1)(l+2) - \sqrt{\dfrac{(l+1)^3(l+2)(2l+3)}{3(2l+1)}}\right]$
$P^2(V_{zz})$	$A_{zz} = (l+1)(l+2)$
$P^2(V_{xz})$	$A_{xz} = -(l+1)/5$
$P^2(V_{xyz})$	$A_{xyz} = \sqrt{A_{xx}^2 + A_{yy}^2 + A_{zz}^2 + A_{xz}^2}$

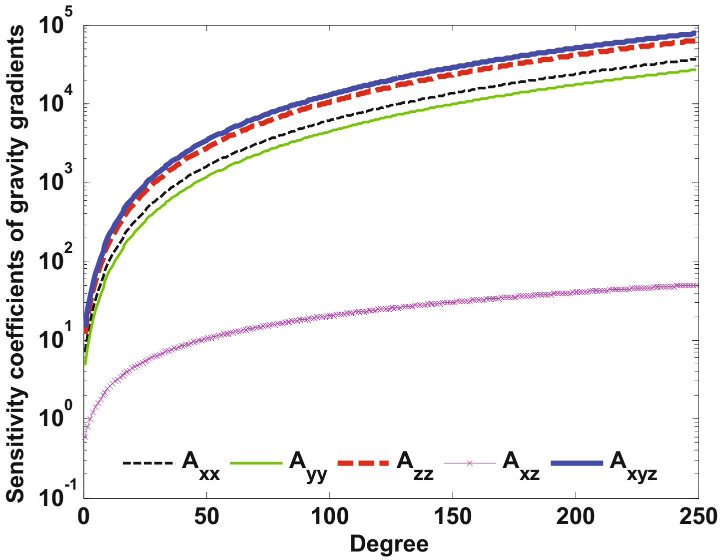

Fig. 2. Sensitivity coefficients $|A_{ij}|$ of power spectrum from satellite gravity gradient tensors at every degree.

Table 2 lists the expressions for sensitivity coefficients $(A_{xx}, A_{yy}, A_{zz}, A_{xz}, A_{xyz})$ of the gravity gradient tensors $(V_{xx}, V_{yy}, V_{zz}, V_{xz}, V_{xyz})$. Figure 2 shows the sensitivity coefficients $|A_{ij}|$ of the gravity gradient tensors at every degree, and the statistical results are displayed in Table 3. The research results are as follows. Firstly, the vertical tensor V_{zz} of the satellite gravity gradients is the uppermost component, which is highly sensitive to the accuracy of the gravity field recovery. Secondly, the horizontal tensors V_{xx}, V_{yy} of the satellite gravity gradients are very important for guaranteeing the accuracy of the Earth's gravitational field measurement. Finally, the cross tensor V_{xz} of the satellite gravity gradients makes a minor contribution to the determination accuracy of the Earth's gravitational field.

Table 3

Statistical results of sensitivity coefficients $\left|A_{ij}\right|$

Parameters	Sensitivity coefficients $\left|A_{ij}\right|$					
	Degree 20	Degree 50	Degree 100	Degree 150	Degree 200	Degree 250
A_{xx}	267	1531	5948	13251	23442	36519
A_{yy}	195	1121	4354	9701	17160	26733
A_{zz}	462	2652	10302	22952	40602	63252
A_{xz}	4	10	20	30	40	50
A_{xyz}	568	6261	12668	28222	49925	77776

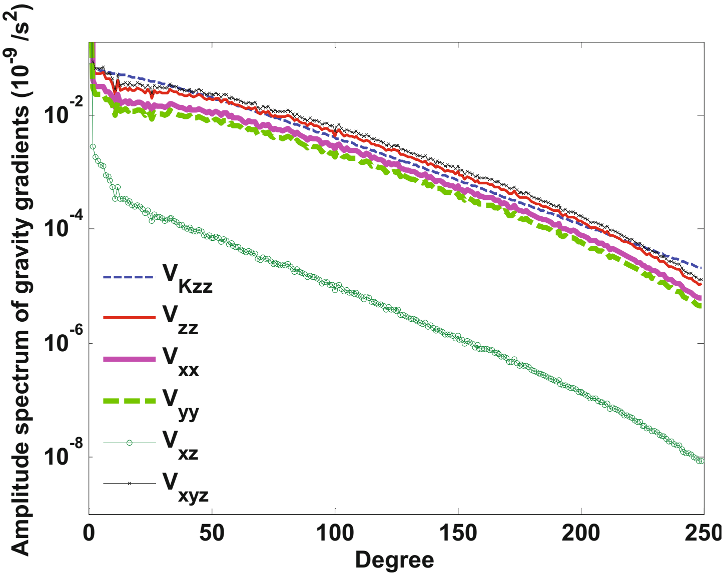

Fig. 3. Signal amplitude spectrum of satellite gravity gradient tensors at every degree.

As illustrated in Fig. 3, the slim dashed, bold solid, bold dashed, and slim solid lines, respectively, represent the signal amplitude spectrum of the Kaula's vertical gravity gradient tensor $V_{\mathrm{K}zz}$ in Eq. 8 and the satellite gravity gradient tensors $(V_{xx}, V_{yy}, V_{zz}, V_{xz}, V_{xyz})$ in Eq. 6, where the orbital altitude of the satellite is $H = 250$ km, the gravitational constant is $GM = 3.986004415 \times 10^{14}$ m^3/s^2, and the mean radius of the Earth is $R_\mathrm{e} = 6378$ km; the statistical results are listed in Table 4. The research results show: (i) the correctness of the power spectrum Eq. 6 of the satellite gravity gradient signals is validated by the conformance of the signal amplitude spectrum between $V_{\mathrm{K}zz}$ and V_{zz}; (ii) the vertical component V_{zz} of the gravity gradient signals is stronger, the horizontal components V_{xx}, V_{yy} of the gravity gradient signals are the second, and the cross component V_{xz} of the gravity gradient signals is weaker; (iii) the diagonal components V_{xx}, V_{yy}, V_{zz} of the gravity gradient tensors are absolutely necessary for precisely mapping the Earth's gravitational field with high spatial resolution.

Table 4

Statistics of signal amplitude spectrum of gravity gradients at every degree

Parameter	Amplitude spectrum of gradient signals [1/s^2]					
	Degree 20	Degree 50	Degree 100	Degree 150	Degree 200	Degree 250
V_{Kzz}	4.692×10^{-11}	2.135×10^{-11}	4.276×10^{-12}	7.579×10^{-13}	1.273×10^{-13}	2.075×10^{-14}
V_{xx}	1.622×10^{-11}	1.192×10^{-11}	3.053×10^{-12}	5.335×10^{-13}	8.196×10^{-14}	6.273×10^{-15}
V_{yy}	1.186×10^{-11}	8.725×10^{-11}	2.235×10^{-12}	3.905×10^{-13}	5.999×10^{-14}	4.592×10^{-15}
V_{zz}	2.807×10^{-11}	2.065×10^{-11}	5.288×10^{-12}	9.239×10^{-13}	1.419×10^{-13}	1.086×10^{-14}
V_{xz}	2.552×10^{-13}	7.941×10^{-14}	1.036×10^{-14}	1.216×10^{-15}	1.405×10^{-16}	8.623×10^{-18}
V_{xyz}	3.452×10^{-11}	2.539×10^{-11}	6.502×10^{-12}	1.136×10^{-12}	1.745×10^{-13}	1.336×10^{-14}

3. ERROR MODELS OF SATELLITE GRAVITY GRADIOMETRY

3.1 Single error model of the gravity gradient

Combining Eqs. 2, 4, and 5, the power spectrum of the satellite gravity gradient tensor error δV_{ij} in the Earth-centered inertial frame is denoted as

$$P^2\left(\delta V_{ij}\right) = \left(\frac{GM}{R_\mathrm{e}^3}\right)^2 \sum_{l=0}^{L} A_{ij}^2 \left(\frac{R_\mathrm{e}}{R_\mathrm{e}+H}\right)^{2l+6} \sum_{m=0}^{l} \left(\delta\bar{C}_{lm}\right)^2 + \left(\delta\bar{S}_{lm}\right)^2 , \tag{9}$$

where $\delta\bar{C}_{lm}, \delta\bar{S}_{lm}$ are the geopotential coefficient errors.

The cumulative geoid height error is defined as

$$\sigma_N = R_\mathrm{e}\sqrt{\sum_{l=2}^{L}\sum_{m=0}^{l}\left(\delta\bar{C}_{lm}\right)^2 + \left(\delta\bar{S}_{lm}\right)^2} . \tag{10}$$

By a combination of Eqs. 9 with 10, the cumulative geoid height error of the satellite gravity gradient tensors is represented as

$$\sigma_N\left(\delta V_{ij}\right)=\frac{R_{\mathrm{e}}^4}{GM\left(\sqrt{T/\Delta t}\right)}\sqrt{\sum_{l=2}^{L}\frac{2l+1}{A_{ij}^2}\left(\frac{R_{\mathrm{e}}+H}{R_{\mathrm{e}}}\right)^{2l+6}\sigma^2\left(\delta V_{ij}\right)}\ , \tag{11}$$

where $\sigma^2(\delta V_{ij})$ is the error variance of the gravity gradient tensors. T is the observation time of the gravity gradient data, Δt is a sampling interval of measurements, and $T/\Delta t$ is the amount of the gravity gradients. According to the fundamental principles of statistics, if the number of the gravity gradient tensors is increased by $T/\Delta t$ times, the recovery accuracy of the Earth's gravitational field should be improved by about $\sqrt{T/\Delta t}$ times.

From Eq. 11 and Table 2, the cumulative geoid height errors of the satellite gravity gradient tensor are shown as

$$\sigma_N\left(\delta V_{xx}\right)=\frac{R_{\mathrm{e}}^4}{GM\left(\sqrt{T/\Delta t}\right)}\sqrt{\sum_{l=2}^{L}\frac{2l+1}{\frac{(l+1)^3(l+2)(2l+3)}{3(2l+1)}}\left(\frac{R_{\mathrm{e}}+H}{R_{\mathrm{e}}}\right)^{2l+6}\sigma^2\left(\delta V_{xx}\right)}, \tag{12}$$

$$\sigma_N\left(\delta V_{yy}\right)=\frac{R_{\mathrm{e}}^4}{GM\left(\sqrt{T/\Delta t}\right)}\sqrt{\sum_{l=2}^{L}\frac{2l+1}{\left[(l+1)(l+2)-\sqrt{\frac{(l+1)^3(l+2)(2l+3)}{3(2l+1)}}\right]^2}\left(\frac{R_{\mathrm{e}}+H}{R_{\mathrm{e}}}\right)^{2l+6}\sigma^2\left(\delta V_{yy}\right)}, \tag{13}$$

$$\sigma_N\left(\delta V_{zz}\right)=\frac{R_{\mathrm{e}}^4}{GM\left(\sqrt{T/\Delta t}\right)}\sqrt{\sum_{l=2}^{L}\frac{2l+1}{(l+1)^2(l+2)^2}\left(\frac{R_{\mathrm{e}}+H}{R_{\mathrm{e}}}\right)^{2l+6}\sigma^2\left(\delta V_{zz}\right)}\ , \tag{14}$$

$$\sigma_N\left(\delta V_{xz}\right)=\frac{R_{\mathrm{e}}^4}{GM\left(\sqrt{T/\Delta t}\right)}\sqrt{\sum_{l=2}^{L}\frac{2l+1}{[(l+1)/5]^2}\left(\frac{R_{\mathrm{e}}+H}{R_{\mathrm{e}}}\right)^{2l+6}\sigma^2\left(\delta V_{xz}\right)}\ , \tag{15}$$

$$\sigma_N\left(\delta V_{xyz}\right)=\frac{R_{\mathrm{e}}^4}{GM\left(\sqrt{T/\Delta t}\right)}\times$$
$$\times\sqrt{\sum_{l=2}^{L}\frac{2l+1}{\frac{(l+1)^3(l+2)(2l+3)}{3(2l+1)}+\left[(l+1)(l+2)-\sqrt{\frac{(l+1)^3(l+2)(2l+3)}{3(2l+1)}}\right]^2+(l+1)^2(l+2)^2+\left[(l+1)/5\right]^2}\left(\frac{R_{\mathrm{e}}+H}{R_{\mathrm{e}}}\right)^{2l+6}\sigma^2\left(\delta V_{xyz}\right)}. \tag{16}$$

3.2 Single error model of orbital position

In the Earth-centered inertial frame, based on the power spectral principle, the power spectrum of the total error δV_{xyz} of the gravity gradient tensor is displayed as

$$P^2\left(\delta V_{xyz}\right)=\left(-\frac{3GM}{r^4}\right)^2\sigma^2(\delta r)\ , \tag{17}$$

where $V_{xyz}=\ddot{r}/r$ is the satellite gravity gradient tensor, and r and $\ddot{r}$ denote the orbital position and centripetal acceleration of the satellite; $\sigma^2(\delta r)$ is the error variance of the satellite orbital position; and $P^2(\delta V_{xyz})$ is given by

$$P^2\left(\delta V_{xyz}\right)=\frac{\sigma^2\left(\delta V_{xyz}\right)}{L_{\max}}\ , \tag{18}$$

where $\sigma^2(\delta V_{xyz})$ is the error variance of the satellite gravity gradient, and $L_{\max}$ is the maximum spherical harmonic degree of the gravity recovery in theory. However, since the high-frequency signals will be submerged into the observation errors, the maximum degree in fact is lower than that in theory

$$L_{\max}=\frac{\pi r}{D}\ , \tag{19}$$

where $D=\dot{r}_0\Delta t$ is the spatial resolution (half-wavelength), and $\dot{r}_0=\sqrt{GM/r}$ is the mean velocity of the satellite.

Combining Eqs. 17-19, the transformational relation between the gravity gradient error δV_{xyz} and the orbital position error δr is denoted as

$$\delta V_{xyz}=\sqrt{\frac{9GM\pi^2}{r^5\Delta t^2}}\delta r\ . \tag{20}$$

Based on Eqs. 16 and 20, the error model of the cumulative geoid height impacted by the orbital position error is shown as

$$\sigma_N(\delta r)=\frac{R_e^4}{GM\left(\sqrt{T/\Delta t}\right)}\times$$
$$\times\sqrt{\sum_{l=2}^{L}\frac{2l+1}{\frac{(l+1)^3(l+2)(2l+3)}{3(2l+1)}+\left[(l+1)(l+2)-\sqrt{\frac{(l+1)^3(l+2)(2l+3)}{3(2l+1)}}\right]^2+(l+1)^2(l+2)^2+\left[(l+1)/5\right]^2}\left(\frac{R_e+H}{R_e}\right)^{2l+6}\sigma^2\left(\sqrt{\frac{9GM\pi^2}{r^5\Delta t^2}}\delta r\right)} \tag{21}$$

3.3 Combined error model between gravity gradient and orbital position

According to Eqs. 16 and 21, the combined error model of the cumulative geoid height affected by the gravity gradient error of the satellite gravity gradiometer and the orbital position error of the GPS/GLONASS receiver is expressed as

$$\sigma_N\left(\delta V_{xyz},\delta r\right)=\frac{R_e^4}{GM\left(\sqrt{T/\Delta t}\right)}\times$$

$$\times\sqrt{\sum_{l=2}^{L}\frac{2l+1}{\frac{(l+1)^3(l+2)(2l+3)}{3(2l+1)}+\left[(l+1)(l+2)-\sqrt{\frac{(l+1)^3(l+2)(2l+3)}{3(2l+1)}}\right]^2+(l+1)^2(l+2)^2+\left[(l+1)/5\right]^2}\left(\frac{R_e+H}{R_e}\right)^{2l+6}\sigma^2(\delta\eta)}\ , \qquad (22)$$

where $\delta\eta=\sqrt{\sigma^2\left(\delta V_{xyz}\right)+\sigma^2\left(\sqrt{\frac{9GM\pi^2}{r^5\Delta t^2}}\delta r\right)}$ is the total error of key instruments from the GOCE satellite, $\sigma^2(\delta V_{xyz})$ is the error variance of the gravity gradient tensors, and $\sigma^2\left(\sqrt{\frac{9GM\pi^2}{r^5\Delta t^2}}\delta r\right)$ is the error variance of the satellite orbital position.

4. RESULTS

4.1 Verification of single and combined error models

As displayed in Fig. 4, the solid, dashed and asterisk lines represent the cumulative geoid height errors impacted by the single gravity gradient error δV_{xyz} of the GOCE gravity gradiometer, the single orbital position error δr of the GPS/GLONASS receiver, and the combined error $\delta(V_{xyz}+r)$, respectively. The statistical results are listed in Table 5, the accuracy indexes of the GOCE key payloads are shown in Table 6, and the related parameters of the error model are represented in Table 7. In terms of the conformity between solid and dashed lines in Fig. 4, we should know that the accuracy indexes of the GOCE key sensors provided by this paper in Table 6 are matched with each other. Additionally, the correctness of the single error model of the satellite gravity gradient (see Eq. 16) and the dependability of the single error model of the satellite orbital position (see Eq. 21) are verified by the conformance of the accuracy indexes from the GOCE key instruments provided by this paper and the ESA. At degree 250, the cumulative geoid height error is 1.769×10^{-1} m based on the combined error model (see Eq. 22) derived

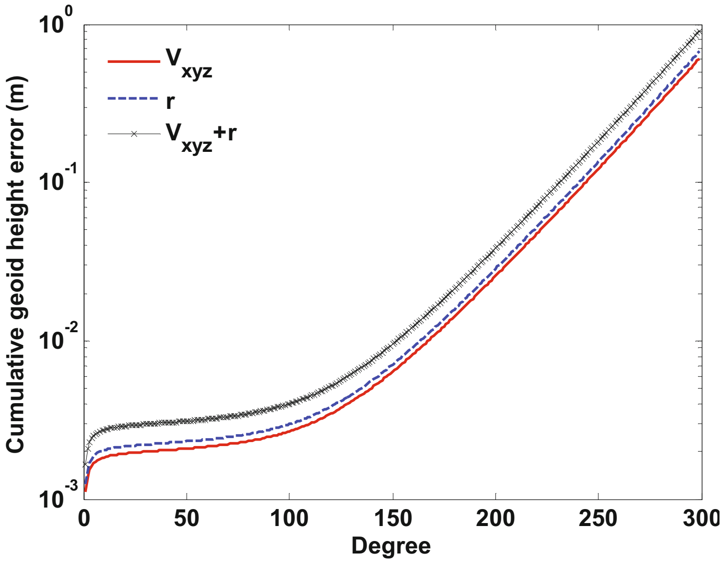

Fig. 4. Cumulative geoid height errors based on the matching measurement accuracies of GOCE spaceborne instrumentations.

Table 5

Statistics of cumulative geoid height error based on the matching accuracy indexes of key payloads

Observation error	Cumulative geoid height error [m]					
	Degree 50	Degree 100	Degree 150	Degree 200	Degree 250	Degree 300
Gravity gradient δV_{xyz}	2.083×10^{-3}	2.660×10^{-3}	6.228×10^{-3}	2.492×10^{-2}	1.185×10^{-1}	6.068×10^{-1}
Orbital position δr	2.310×10^{-3}	2.950×10^{-3}	2.906×10^{-3}	2.765×10^{-2}	1.313×10^{-1}	6.730×10^{-1}
Combined model $\delta(V_{xyz}+r)$	3.110×10^{-3}	3.972×10^{-3}	9.299×10^{-3}	3.722×10^{-2}	1.769×10^{-1}	9.062×10^{-1}

from the gravity gradient error and the orbital position error, which preferably accords with the measurement accuracy of 1.760×10^{-1} m from the Earth gravity field model GO_CONS_GCF_2_TIM_R2. Therefore, the combined error model established by this study is correct.

Table 6

Matching accuracy indexes of GOCE spaceborne instruments

Observations	Accuracy indexes
Gravity gradient	3×10^{-12} /s^2
Orbital position	1×10^{-2} m

Table 7

Related parameters of GOCE error models

Parameters	Indexes
Orbital altitude H	250 km
Earth's radius R_e	6370 km
Observation time T	8 months
Sampling interval Δt	5 s
Gravitational constant GM	$3.986004415 \times 10^{14}$ m^3/s^2

4.2 Requirements analysis for GOCE Follow-On mission

4.2.1 Impact of observation error in gravity gradient

As illustrated in Fig. 5, the cumulative geoid height errors from GOCE Follow-On up to degree 300 are estimated based on different measurement accuracies of 3×10^{-12} /s^2, 3×10^{-13} /s^2, 3×10^{-14} /s^2, and 3×10^{-15} /s^2 from the satellite gravity gradients using the single error model of the gravity gradient (see Eq. 16, Tables 6 and 7), respectively. At degree 300, the cumulative geoid height error is 6.068×10^{-1} m using the gravity gradient error of 3×10^{-12} /s^2. If the measurement accuracies of the gravity gradient are designed as 3×10^{-13} /s^2, 3×10^{-14} /s^2, and 3×10^{-15} /s^2, the cumulative geoid height errors will be improved by 10 times, 100 times, and 1000 times, respectively. The geophysical analysis is described as follows. The measurement precision of the space-borne gravity gradiometer plays a very significant part in improving the recovery accuracy of the Earth's gravitational field. Therefore, if the cold-atom interferometric gradiometer is used in the next-generation satellite gravity mission from GOCE Follow-On with a measurement accuracy of 10^{-13}-10^{-15} /s^2 (Yu *et al*. 2006, Johnson 2011), the determination accuracy of the Earth's gravitational field from the future GOCE Follow-On satellite is at least 10 times higher than that from the current GOCE satellite.

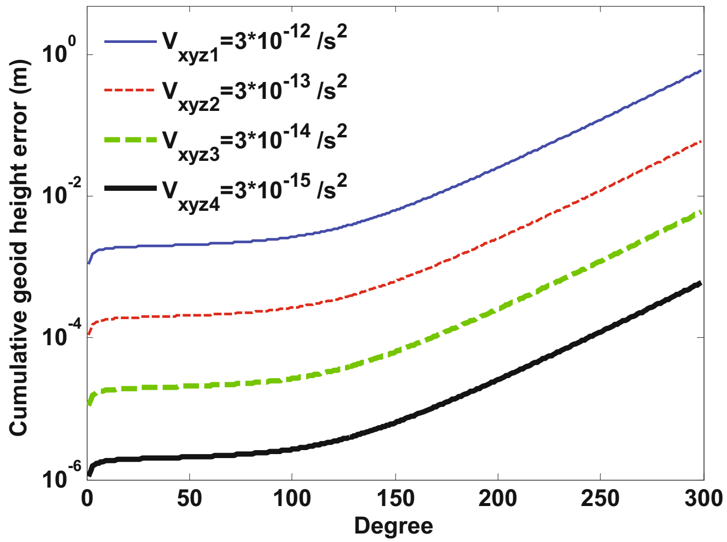

Fig. 5. Cumulative geoid height errors based on different measurement accuracies of satellite gravity gradients.

4.2.2 Influence of measurement accuracy of orbital position

Figure 6 displays the GOCE Follow-On cumulative geoid height error up to degree 300 using the measurement accuracies of 10^{-2}, 10^{-3}, 10^{-4}, and 10^{-5} m

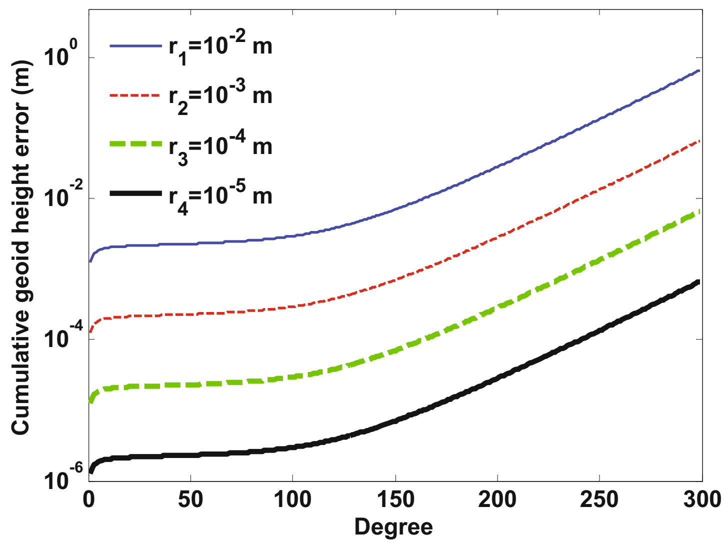

Fig. 6. Cumulative geoid height errors based on different measuring accuracies of satellite orbital position.

for the orbital position of the satellite by the single error model of the orbital position (see Eq. 21, Tables 6 and 7). At degree 300, the cumulative geoid height error is 6.730×10^{-1} m using an orbital accuracy of 10^{-2} m, and the cumulative geoid height errors are linearly improved while the measurement accuracies of the satellite orbital position are enhanced by 10 times, 100 times, and 1000 times, respectively. The geophysical analysis is depicted as follows. The satellite gravity gradiometry is less sensitive to the precise orbit determination of the satellite and the orbital accuracy of the Global Navigation Satellite System (GNSS) (*e.g.*, GPS, GLONASS, Compass, Galileo, *etc.*) is about cm-level. Therefore, the measurement accuracy of the satellite orbital position from the future GOCE Follow-On mission is preferable for 1-0.1 cm.

4.2.3 Effect of orbital altitude of satellite

As illustrated in Fig. 7, the bold solid, bold dashed, slim dashed, and slim solid lines, respectively, represent the cumulative geoid height errors up to degree 300 by different satellite orbital altitudes of 200, 250, 300, and 350 km based on the GOCE Follow-On combined error model (see Eq. 22, Tables 6 and 7), and the statistical results are listed in Table 8. At degree 300, the cumulative geoid height error is 1.049×10^{-1} m with an orbital altitude of 200 km. If the GOCE Follow-On satellite operates at the orbital altitudes of 250, 300, and 350 km, the cumulative geoid height errors are reduced by 8.639 times, 75.491 times, and 660.819 times, respectively. The

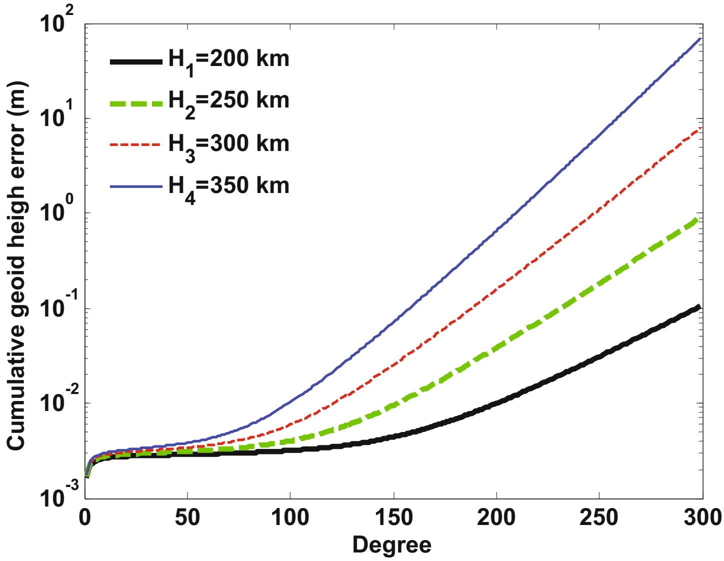

Fig. 7. Cumulative geoid height errors using different satellite orbital altitudes.

Table 8

Statistical results of impacts of different orbital altitudes on cumulative geoid height error

Orbital altitude [km]	Cumulative geoid height error [m]					
	Degree 50	Degree 100	Degree 150	Degree 200	Degree 250	Degree 300
$H_1 = 200$	2.885×10^{-3}	3.170×10^{-3}	4.366×10^{-3}	9.776×10^{-3}	3.025×10^{-2}	1.049×10^{-1}
$H_2 = 250$	3.110×10^{-3}	3.972×10^{-3}	9.299×10^{-3}	3.722×10^{-2}	1.769×10^{-1}	9.062×10^{-1}
$H_3 = 300$	3.403×10^{-3}	5.816×10^{-3}	2.448×10^{-2}	1.512×10^{-1}	1.058×10^{0}	7.919×10^{0}
$H_4 = 350$	3.800×10^{-3}	9.882×10^{-3}	6.836×10^{-2}	6.238×10^{-1}	6.360×10^{0}	6.932×10^{1}

geophysical analysis is recounted as follows. Because the Earth's gravitational potential presents a tendency of the exponential attenuation with increasing the orbital altitude of the satellite, the lower orbital altitude makes a great contribution to substantially improve the accuracy of the Earth's gravitational field determination. However, the atmospheric drag acting on the satellite will be enhanced by one order of magnitude with the decrease in the orbital altitude by per 100 km. Therefore, although the GOCE Follow-On satellite carries the drag-free control system, the optimal design of the satellite orbital altitude is very crucial all the time. To sum up, we suggest that it is suitable for selecting the orbital altitude range of 200-250 km.

4.2.4 Gravity recovery from GOCE Follow-On

As illustrated in Fig. 8, the dashed line represents the GOCE-only Earth gravity field model GO_CONS_GCF_2_TIM_R2 complete up to degree and order 250 released by the TUM, Germany, and the cumulative geoid height error is 1.760×10^{-1} m at degree 250. The solid line denotes the cumulative geoid height error up to degree 400 from the future GOCE Follow-On mission by the combined error model (see Eq. 22), based on the gravity gradient error of 3×10^{-13} /s^2, orbital position error of 0.1 cm and orbital altitude of 200 km, and adopting an observation period of 8 months and a 5-s sampling interval. The statistical results of the cumulative geoid height errors are displayed in Table 9. The reasons why the accuracy of the Earth's gravitational field based on the future GOCE Follow-On mission is improved by a factor of more than 10 as compared with that based on the current GOCE mission are expatiated as follows.

Firstly, the orbital altitude of the future GOCE Follow-On satellite (200 km) is lower than that of the current GOCE satellite (250 km). Hence, the negative effects on the signal attenuation of gravity information with the increase in the orbital altitude are propitious to be mitigated to a great extent by the future GOCE Follow-On satellite.

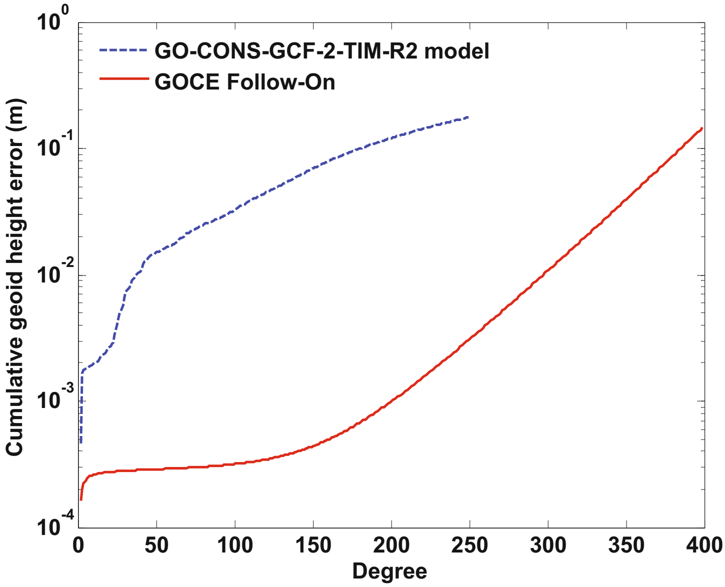

Fig. 8. A comparison of cumulative geoid height errors between the current GOCE and future GOCE Follow-On satellites.

Table 9

Statistical results of cumulative geoid height errors from GOCE and GOCE Follow-On

Gravity satellites	Cumulative geoid height error [m]							
	Degree 50	Degree 100	Degree 150	Degree 200	Degree 250	Degree 300	Degree 350	Degree 400
GO_CONS_GCF_2_TIM_R2	1.493×10^{-2}	3.225×10^{-2}	6.881×10^{-2}	1.198×10^{-1}	1.760×10^{-1}	–	–	–
GOCE Follow-On	1.493×10^{-4}	3.171×10^{-4}	4.366×10^{-4}	9.776×10^{-4}	3.025×10^{-3}	1.049×10^{-2}	3.843×10^{-2}	1.458×10^{-1}

Secondly, the measurement accuracy of the space-borne instruments (*e.g.*, cold-atom interferometric gravity gradiometer) from GOCE Follow-On is at least one order of magnitude higher than that (*e.g.*, electrostatic suspension gravity gradiometer) from GOCE. Herewith, the accuracy of the Earth's gravitational field from GOCE Follow-On is conducive to be substantially improved due to an optimum Signal-to-Noise Ratio (SNR) of the satellite observations.

5. CONCLUSION

The core objectives of this investigation are to establish the recovery error model of the satellite gravity gradiometry through the power spectral principle and perform the requirements analysis for the future GOCE Follow-On mission. The summary of the concrete results is stated as follows.

Firstly, we developed the single and combined error models aiming at availably and rapidly estimating the accuracy of the gravity field by adopting the errors in gravity gradient and orbital position.

- We demonstrated the matching relationship of the measurement accuracies from the GOCE space-borne sensors making use of the single error model, and proved the reliability of the single error model by the measurement accuracy of this study in accordance with that of ESA.
- We validated the dependability of the combined error model. At degree 250, the cumulative geoid height error of this study basically tallies with that of the existing GO_CONS_GCF_2_TIM_R2 model.

Secondly, we implemented the sensitivity analysis for the next-generation GOCE Follow-On system regarding different measurement accuracies of the gravity gradient, different observation errors in the orbital position, and different orbital altitudes of the satellite.

- The recovery accuracy of the Earth's gravitational field from GOCE Follow-On is at lowest 10 times superior to that from GOCE if the cold-atom interferometric gradiometer is applied in the future GOCE Follow-On satellite. Accordingly, it is a preferred choice for the measurement accuracy of 10^{-13}-10^{-15} /s^2 of the gravity gradient in the next-generation GOCE Follow-On mission.
- Because the satellite gravity gradiometry measurement has a low sensitivity to the observation accuracy of the orbital position and the topmost precision of the GPS, GLONASS, Compass, and Galileo orbit determination is just cm-level at present, an orbital accuracy of 1-0.1 cm is an optimal design for the future GOCE Follow-On system.
- The signal strength of the Earth's gravitational field is apt to be weakened with the increase in the orbital altitude of the satellite, and the adverse influences of the non-conservation force will be sharply added with reducing the orbital altitude at the same time. Consequently, the future GOCE Follow-On satellite had better operate at an orbital altitude of 200-250 km.
- The accuracy of the gravity recovery from the future GOCE Follow-On satellite sufficiently surpasses the current GOCE satellite on account of the lower orbital altitude of the satellite and the higher observation accuracy of the key payloads.

Acknowledgments. We greatly appreciate the helpful suggestions from editors and anonymous reviewers. This work was supported by the Main Direction Program of Knowledge Innovation of Chinese Academy of Sciences for Distinguished Young Scholar (Grant No. KZCX2-EW-QN114), the National Natural Science Foundation of China (Grant Nos. 41574014, 41131067, 11572168, 11173049, 41274041, and 41404019), the Merit-based Scientific Research Foundation of the State Ministry of Human Resources and Social Security of China for Returned Overseas Chinese Scholars (Grant No. 201101), the Open Research Fund Program of the Key Laboratory of Geospace Environment and Geodesy, Ministry of Education, China (Grant No. 11-01-02), the Open Research Fund Program of the Key Laboratory of Geo-Informatics of National Administration of Surveying, Mapping and Geoinformation of China (Grant No. 201322), the Open Research Fund Program of the State Key Laboratory of Geo-information Engineering, China (Grant No. SKLGIE2013-M-1-5), the Main Direction Program of Institute of Geodesy and Geophysics, Chinese Academy of Sciences (Grant No. Y309451045), the Research Fund Program of State Key Laboratory of Geodesy and Earth's Dynamics, China (Grant No. Y309491050), the Research Fund of the National Civilian Space Infrastructure Project (Grant No. Y419341034), and the Research Fund of the Lu Jiaxi Young Talent and the Youth Innovation Promotion Association of Chinese Academy of Science (Grant No. Y305171017).

References

Bender, P.L., R.S. Nerem, and J.M. Wahr (2003), Possible future use of laser gravity gradiometers, *Space Sci. Rev.* **108**, 1-2, 385-392, DOI: 10.1023/A:1026100130397.

Bian, S.F., and B. Ji (2006), The development and application of the gravity gradiometer, *Prog. Geophys.* **21**, 660-664 (in Chinese).

Bobojć, A., and A. Drożyner (2011), GOCE satellite orbit in the aspect of selected gravitational perturbations, *Acta Geophys.* **59**, 2, 428-452, DOI: 10.2478/s11600-010-0052-3.

Bruinsma, S.L., J.C. Marty, G. Balmino, R. Biancale, C. Foerste, O. Abrikosov, and H. Neumayer (2010), GOCE gravity field recovery by means of the direct numerical method. **In:** *Proc. ESA Living Planet Symposium, 27 June – 2 July 2010, Bergen, Norway*.

Ditmar, P., R. Klees, and F. Kostenko (2003), Fast and accurate computation of spherical harmonic coefficients from satellite gravity gradiometry data, *J. Geodesy* **76**, 11-12, 690-705, DOI: 10.1007/s00190-002-0298-x.

Eshagh, M. (2010), Alternative expressions for gravity gradients in local north-oriented frame and tensor spherical harmonics, *Acta Geophys.* **58**, 2, 215-243, DOI: 10.2478/s11600-009-0048-z.

Eshagh, M. (2011), On integral approach to regional gravity field modelling from satellite gradiometric data, *Acta Geophys.* **59**, 1, 29-54, DOI: 10.2478/s11600-010-0033-6.

Goiginger, H., E. Höck, D. Rieser, T. Mayer-Gürr, A. Maier, S. Krauss, R. Pail, T. Fecher, T. Gruber, J.M. Brockmann, I. Krasbutter, W.-D. Schuh, A. Jäggi, L. Prange, W. Hausleitner, O. Baur, and J. Kusche (2011), The combined satellite-only global gravity field model GOCO02S. **In:** *Proc. 2011 General Assembly of the European Geosciences Union, 4-8 April 2011, Vienna, Austria*.

Hsu, H.T. (2001), Satellite gravity missions – new hotpoint in geodesy, *Sci. Surv. Mapp.* **26**, 1-3 (in Chinese).

Jenkins, G.M., and D.G. Watts (1968), *Spectral Analysis and Its Applications*, Holden-Day, San Francisco.

Johnson, D.M.S. (2011), Long baseline atom interferometry, Ph.D. Thesis, Stanford University, Department of Physics, Stanford, USA, 1-142.

Kaula, W.M. (1966), *Theory of Satellite Geodesy*, Blaisdell Publ. Co., Waltham.

Liu, X.G., Z.X. Pang, and J. Wu (2012), Earth's gravitational field model determination from different types of gravimetric data based on iteration method, *Prog. Geophys.* **27**, 6, 2342-2347, DOI: 10.6038/j.issn.1004-2903.2012.06.009.

Meng, J.C., and S.Y. Liu (1993), Research on accuracies for satellite gravity gradiometry and Earth's gravitational field, *Chin. J. Geophys.* **36**, 725-739 (in Chinese).

Migliaccio, F., M. Reguzzoni, F. Sansò, C.C. Tscherning, and M. Veicherts (2010), GOCE data analysis: the space-wise approach and the first space-wise gravity field model. **In:** *Proc. ESA Living Planet Symposium, 27 June – 2 July 2010, Bergen, Norway*.

Migliaccio, F., M. Reguzzoni, A. Gatti, F. Sansò, and M. Herceg (2011), A GOCE-only global gravity field model by the space-wise approach. **In:** *Proc. 4th Int. GOCE User Workshop, European Geosciences Union (EGU), Vienna, Austria*.

Milani, A., A. Rossi, and D. Villani (2005), A timewise kinematic method for satellite gradiometry: GOCE simulations, *Earth Moon Planets* **97**, 1-2, 37-68, DOI: 10.1007/s11038-005-9042-x.

Moritz, H. (1971), Kinematic geodesy II, Rep. 165, Department of Geodetic Science, The Ohio State University, Columbus, USA.

Pail, R., H. Goiginger, R. Mayrhofer, W.D. Schuh, J.M. Brockmann, I. Krasbutter, E. Höck, and T. Fecher (2010), GOCE gravity field model derived from orbit and gradiometry data applying the time-wise method. **In:** *Proc. ESA Living Planet Symp., 28 June – 2 July 2010, Bergen, Norway*, ESA SP-686.

Pail, R., A. Albertella, and H. Goiginger (2011a), Time-wise global GOCE gravity field models and their use for modelling ocean circulation. **In:** *Proc. 25th General Assembly of International Union of Geodesy and Geophysics (IUGG) "Earth on the Edge: Science for a Sustainable Planet", 27 June – 8 July 2011, Melbourne, Australia*.

Pail, R., S. Bruinsma, F. Migliaccio, C. Förste, H. Goiginger, W.-D. Schuh, E. Höck, M. Reguzzoni, J.M. Brockmann, O. Abrikosov, M. Veicherts, T. Fecher, R. Mayrhofer, I. Krasbutter, F. Sansò, and C.C. Tscherning (2011b), First GOCE gravity field models derived by three different approaches, *J. Geodesy* **85**, 11, 819-843, DOI: 10.1007/s00190-011-0467-x.

Pertusini, L., M. Reguzzoni, and F. Sansò (2010), Analysis of the covariance structure of the GOCE space-wise solution with possible applications. **In:** S.P. Mertikas (ed.), *Gravity, Geoid and Earth Observation, IAG Commission 2: Gravity Field, Chania, Crete, Greece, 23-27 June 2008*, International Association of Geodesy Symposia, Vol. 135, Springer, Berlin Heidelberg, 195-202.

Press, W.H., B.P. Flannery, S.A. Teukolsky, and W.T. Vetterling (1992a), Power spectra estimation using the FFT. **In:** W.H. Press, B.P. Flannery, S.A. Teukolsky, and W.T. Vetterling, *Numerical Recipes in Fortran 77: The Art of Scientific Computing*, 2nd ed., Cambridge University Press, Cambridge, 542-551.

Press, W.H., B.P. Flannery, S.A. Teukolsky, and W.T. Vetterling (1992b), Power spectrum estimation by the maximum entropy (all poles) method. **In:** W.H. Press, B.P. Flannery, S.A. Teukolsky, and W.T. Vetterling, *Numerical Recipes in Fortran 77: The Art of Scientific Computing*, 2nd ed., Cambridge University Press, Cambridge, 565-569.

Reguzzoni, M., and N. Tselfes (2009), Optimal multi-step collocation: application to the space-wise approach for GOCE data analysis, *J. Geodesy* **83**, 1, 13-29, DOI: 10.1007/s00190-008-0225-x.

Reguzzoni, M., A. Gatti, F. Migliaccio, and M. Veicherts (2010), The space-wise approach for the computation of a GOCE-only gravity field solution. **In:** Proc. American Geophysical Union (AGU), Fall Meeting 2010, Abstr. G33B-04.

Rummel, R. (2003), How to climb the gravity wall, *Space Sci. Rev.* **108**, 1-2, 1-14, DOI: 10.1023/A:1026206308590.

Sanso, F., A. Gatti, and F. Migliaccio (2011), A space-wise gravity field model from one year of GOCE data. **In:** *Proc. 25th General Assembly of International Union of Geodesy and Geophysics (IUGG) "Earth on the Edge: Science for a Sustainable Planet", 27 June – 8 July 2011, Melbourne, Australia*.

Tscherning, C.C. (1976), Computation of the second-order derivatives of the normal potential based on the representation by a Legendre series, *Manuscr. Geod.* **1**, 71-92.

van Gelderen, M., and R. Koop (1997), The use of degree variances in satellite gradiometery, *J. Geodesy* **71**, 6, 337-343, DOI: 10.1007/s001900050101.

Welch, P.D. (1967), The use of fast Fourier transform for the estimation of power spectra: a method based on time averaging over short, modified periodograms, *IEEE Trans. Audio Electroacoust.* **AU-15**, 70-73.

Yu, N., J.M. Kohel, J.R. Kellogg, and L. Maleki (2006), Development of an atom-interferometer gravity gradiometer for gravity measurement from space, *Appl. Phys. B* **84**, 4, 647-652, DOI: 10.1007/s00340-006-2376-x.

Zheng, W., H.T. Hsu, M. Zhong, and M.J. Yun (2011a), Efficient calibration of the non-conservative force data from the space-borne accelerometers of the twin GRACE satellites, *Trans. Jpn. Soc. Aeronaut. Space Sci.* **54**, 184, 106-110, DOI: 10.2322/tjsass.54.106.

Zheng, W., H.T. Hsu, M. Zhong, and M.J. Yun (2011b), Accurate and rapid determination of GOCE Earth's gravitational field using time-space-wise approach associated with Kaula regularization, *Chin. J. Geophys.* **54**, 1, 14-21, DOI: 10.1002/cjg2.1581.

Zheng, W., H.T. Hsu, M. Zhong, and M.J. Yun (2012a), Efficient accuracy improvement of GRACE global gravitational field recovery using a new Inter-satellite Range Interpolation Method, *J. Geodyn.* **53**, 1-7, DOI: 10.1016/j.jog.2011.07.003.

Zheng, W., H.T. Hsu, M. Zhong, and M.J. Yun (2012b), Precise recovery of the Earth's gravitational field with GRACE: Intersatellite Range-Rate Interpolation Approach, *IEEE Geosci. Remote Sens. Lett.* **9**, 3, 422-426, DOI: 10.1109/LGRS.2011.2171475.

Zheng, W., H.T. Hsu, M. Zhong, and M.J. Yun (2012c), A contrastive study on the influences of radial and three-dimensional satellite gravity gradiometry on the accuracy of the Earth's gravitational field recovery, *Chin. Phys. B* **21**, 10, 109101-1–109101-8, DOI: 10.1088/1674-1056/21/10/109101.

Zheng, W., H.T. Hsu, M. Zhong, C.S. Liu, and M.J. Yun (2013), Efficient and rapid accuracy estimation of the Earth's gravitational field from next-generation GOCE Follow-On by the analytical method, *Chin. Phys. B* **22**, 4, 049101-1–049101-8, DOI: 10.1088/1674-1056/22/4/049101.

Zheng, W., H.T. Hsu, M. Zhong, and M.J. Yun (2015a), Requirements analysis for future satellite gravity mission Improved-GRACE, *Surv. Geophys.* **36**, 1, 87-109, DOI: 10.1007/s10712-014-9306-y.

Zheng, W., H.T. Hsu, M. Zhong, and M.J. Yun (2015b), Sensitivity analysis for key payloads and orbital parameters from the next-generation Moon-Gradiometer satellite gravity program, *Surv. Geophys.* **36**, 1, 111-137, DOI: 10.1007/s10712-014-9310-2.

Received 19 August 2013
Received in revised form 31 October 2014
Accepted 6 March 2015